Proceedings of Proceedings of the ASME 2022 International Technical Conference and Exhibition on Packaging and Integration of Electronic and Photonic Microsystems InterPACK2022
October 25-27, 2022, Garden Grove, California, USA

InterPack2022-98066

TOPOLOGY OPTIMIZATION OF HEAT SINK FOR 3D INTEGRATED POWER CONVERTERS

Xiaoqiang Xu[1], Abdul Basit Mirza[2], Lingfeng Gao[1], Fang Luo[1], Shikui Chen[1]*
[1]Department of Mechanical Engineering,
[2]Department of Electrical and Computer Engineering
State University of New York at Stony Brook, Stony Brook, NY 11794, USA

ABSTRACT

This paper proposes a density-based topology optimization scheme to design a heat sink for the application of a 3D integrated SIC-based 75 kVA Intelligent Power Stage (IPS). The heat sink design considers the heat conduction and convection effects with forced air cooling. The objective function is to minimize the thermal compliance of the whole structure. A volume constraint is imposed to reduce the overall volume of the designed heat sink to make it conformal to the underlying power devices. Some numerical techniques like filtering and projection schemes are employed to render a crisp design. Some 2D benchmarks examples are first provided to demonstrate the effectiveness of the proposed method. Then a 3D heat sink, especially designed for the 3D IPS, is topologically optimized. The classic tree-like structure is reproduced to reinforce the convection effect. Some comparisons with the intuitive baseline designs are made through numerical simulation. The optimized heat sinks are shown to provide a more efficient cooling performance for the 3D integrated power converter assembly.

1 INTRODUCTION

Recent years have witnessed a trend that the power devices are made with a higher power density and yet a more compact configuration. In order to extend the lifespan of such power devices, efficient thermal management becomes critical to maintain a moderate temperature field by dissipating the heat loss in a timely manner [1]. The design of heat sink has long been an extensively studied topic [2–4]. The most commonly used cooling is the natural convection [5], often with air flow. The convection coefficient, however, is relatively low for such cooling mechanism, making it less suitable for high-power-density devices heat dissipation. Another popular method is to employ forced convection [6], which often involves some coolant, e.g., water. For such heat sink systems, the design for an efficient fluid channel is critical. Beside trying to dissipate the heat loss of the power devices promptly in a certain way, researchers have also attempted to recycle this portion of energy using thermoelectric effect [7–9]. In the field of electrical engineering, a number of endeavors have been devoted into the design for heat sinks. For example, Hensler et al. [10] studies the SiC three level inverter with high power density for industrial applications using forced air cooling. Chen et al. [11] optimized a three-sided cooling by varying the number and distribution of cylindrical holes. The above works usually start with some baseline designs and conduct a parametric study to find a better performer.

Topology optimization, which devotes to finding the optimal material distribution for a desired performance, has been an ideal tool for designing the thermal management devices [2, 12–14]. One unique thing about topology optimization is that it can give you designs out of your intuition, i.e., generative designs. Some notable research works on heat sink designs from topology optimization community are summarized here. Dede [15] provided an easy-to-use COMSOL/MATLAB implementation of topology optimization of heat transfer and fluid flow system. In one of his

*Address all correspondence to this author.

subsequent works, Dede et al. [16] came up with a 3D heat sink and compared its performance with some intuitive baseline designs. Koga et al. [2] studied the heat sink design for small scale fluid flow systems with a multi-objective function that combines pressure drop minimization and heat transfer maximization. The topology optimization of heat sinks cooled by natural convection was investigated in [5, 17, 18]. In [19–21] , the heat sink designs were not only topologically optimized, but also experimentally realized to validate their cooling performance.

However, the topology optimization attempts on the power devices have not been quite rich. In this study, we apply the density-based topology optimization method to design thermal heat sinks for the 3D integrated power stages (IPS). The convection effect is taken into consideration by treating it as an equivalent volumetric integral term. The topologically optimized 3D thermal heat sink is made conformal to the underlying IPS architecture. Its cooling performance are investigated through the comparisons of the FEA with two baseline designs with varying number of holes with a fixed diameter. The optimized heat sink has a superior cooling performance compared with the two intuitive baseline designs.

This paper is organized as follows: Section 2 will provide governing equation for this optimization problem. Topology optimization formulation will be detailed in Section 3. Two numerical examples are given in Section 4. Section 5 will end with conclusion and future work.

2 GOVERNING EQUATIONS

In a PDE-constrained topology optimization method, the physics governing equation will be solved at each iteration to evaluate the performance of the current design. In this paper, we consider the thermal conduction and convection phenomena simultaneously under the steady-state condition. All the material properties are assumed to be isotropic. The equations governing the thermal conduction and convection phenomena are given as follows:

$$
\begin{aligned}
&-k\nabla^2 T = b, \ in \ \Omega \\
&k\nabla T \cdot \mathbf{n} = q, \ on \ \Gamma_N \\
&k\nabla T \cdot \mathbf{n} = 0, \ on \ \Gamma_H \\
&k\nabla T \cdot \mathbf{n} + h(T - T_\infty) = 0, \ on \ \Gamma_C \\
&T = T_0, \ \ on \ \Gamma_D
\end{aligned}
\tag{1}
$$

where k is the thermal conductivity; T is the state variable temperature; b is the rate of internal heat generation; $\mathbf{n}$ is the outward unit normal vector of the structural boundary; q is the heat flux in the inward normal direction; T_∞ is the ambient temperature and h is the thermal convection coefficient . As shown in Figure 1, the structural boundaries of the design domain Ω are composed of a Dirichlet boundary Γ_D with $T = T_0$, a homogeneous Neumann boundary Γ_H which is adiabatic, a non-homogeneous Neumann boundary Γ_N with a heat flux q, and a convection boundary Γ_C. The existence of thermal convection makes this heat sink design a typical design-dependent optimization problem, since the convection only happens on the interface between the solid and air flow. As our design variable, the shape and topology of the solid structure will be evolved iteratively, resulting in a constantly changing interface between solid region and the cooling medium air flow.

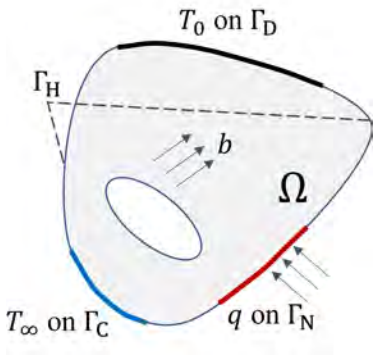

FIGURE 1: THE DIAGRAM OF A THERMAL CONDUCTOR CONSIDERING CONVECTION EFFECT

3 TOPOLOGY OPTIMIZATION FORMULATION OF THE HEAT SINK

In this study, we employ the density-based topology optimization [22–24] to design a conformal heat sink for the power device. In the classic solid isotropic material with penalization (SIMP) method, each finite element or mesh node is assigned with a pseudo density ρ, which takes the value from interval 0 to 1. The continuous design variable ρ is relaxed from the original discrete 0-1 optimization problem, which suffers from numerical issues and could not utilize the gradient-based algorithms [25]. The evolution of shape and topology of the design can be realized by updating the design variable ρ according to the shape sensitivity analysis, a feature of the physics-driven optimization.

Here, we present the problem-setting for a heat sink design. The strong form governing equation (1) can be transformed into weak form by first multiplying a test function $\bar{T}$, integrating over the whole domain, utilizing the product rule and applying the 2D divergence theorem with the aforementioned boundary conditions mentioned in Section 2. The weak form equation

considering the convection effect can be given as follows [16] :

$$a(T,\bar{T}) = l(\bar{T}),\ \forall \bar{T} \in U_{ad} \tag{2}$$

where $\bar{T}$ is the test function for the temperature and U_{ad} is the space of the virtual temperature field meeting the same boundary condition as described in Section 2 . The bilinear function at the left side of equation (2) is defined as:

$$a(T,\bar{T}) = \int_{\Omega} k\nabla T \cdot \nabla \bar{T} d\Omega. \tag{3}$$

The linear function at the right side of equation (2) is defined as:

$$l(\bar{T}) = \int_{\Omega} b\bar{T} d\Omega + \int_{\Gamma_N} q\bar{T} ds + \int_{\Gamma_C} h(T_{\infty} - T)\bar{T} ds. \tag{4}$$

The thermal convection actually only happens on the interface between two phases, e.g., aluminum and air flow, which requires the detection of the structural boundaries to enforce the design-dependent convection load constantly. As in the shape and topology optimization, the self design variable is essentially the shape and topology of a candidate design, characterized by the structural boundaries between different phases, which is challenging to keep track of in real time. To overcome this hurdle, the last term in equation (4) is modified into a volume integral [16, 26] as follows:

$$l(\bar{T}) = \int_{\Omega} b\bar{T} d\Omega + \int_{\Gamma_N} q\bar{T} ds + \int_{\Omega} h(\rho)(T_{\infty} - T)\bar{T} ds. \tag{5}$$

where $h(\rho)$ is the thermal convection coefficient, defined as a function of the density variable ρ. The piece-wise function $h(\rho)$ is defined as follows [16]:

$$h(\rho) = \begin{cases} h_0 \times 10^{-2} & \text{if } \rho < \rho_l \\ h_0 & \text{if } \rho_l \leq \rho \leq \rho_u \\ 0 & \text{if } \rho_u < \rho, \end{cases} \tag{6}$$

where h_0 is the reference thermal convection coefficient, which will be applied on the interface between the solid material and the coolant phase, e.g., air flow. ρ_l and ρ_u are the lower and upper limit, respectively, for density variable ρ, which is used to roughly identify the boundary between the solid material and air flow. When the density variable ρ is smaller than the lower threshold ρ_l, it means there will be air at that region and a much smaller thermal convection coefficient will be applied to avoid numerical instability. When ρ is larger than the upper threshold ρ_u, it indicates that the whole local region is occupied by solid material, where the thermal convection will not occur, resulting in $h_0 = 0$. This treatment elegantly circumvents the difficulty in implementing the integral on boundaries, which are dynamically changing as the optimization process goes on.

The formal problem-setting for the heat sink design is given as follows:

$$\begin{aligned} \underset{\rho}{Inf} \quad & J = \int_{\Omega} \frac{1}{2} \cdot k \cdot (\nabla T)^2 \Omega, \\ S.t. \quad & a(T,\bar{T}) = l(\bar{T}),\ \forall \bar{T} \in U_{ad} \\ & V(\Omega) \leq V^*, \end{aligned} \tag{7}$$

where $V(\Omega)$ the volume of the current solid domain, V^* is the volume upper constraint since the heat sink needs to be compact and lightweight. The influence of objective function selection on the heat sink design using topology optimization has been investigated in [27]. According to the findings in [27], minimizing the thermal compliance objective function J is equivalent to minimizing the thermal resistance of the system, provided that a constant boundary heat flux is enforced and the thermal conductivity of the solid material is high. The physics meaning of minimizing this objective function J is to minimize the mean temperature of the design domain.

Some numerical techniques [28, 29] are often employed in the density-based topology optimization to regulate the optimization problem, avoid numerical instability and render a crisp "0-1" design, i.e., avoiding intermediate densities in the final optimized designs, which does not make physical sense. To be specific, the raw design variable ρ_c is assigned to each mesh node ranging continuously from 0 to 1. A regularization scheme is applied through the Helmholtz equation [28] as follows:

$$\rho_f = R_{min}^2 \nabla^2 \rho_f + \rho_c, \tag{8}$$

where ρ_f is the filtered density variable. The R_{min} is introduced to enforce a minimum length scale with a default value equal

to the mesh edge size. Although this filtering process can effectively remove the mesh dependence, it tends to generate "grey region", where the filtered density variable ρ_f takes the value between 0 and 1, say, 0.5. A density of 0.5 does not make sense physically and is not desired during the optimization process. The projection scheme [29] will then come into play by pushing the intermediate densities toward 0 or 1. The projection scheme is based on the hyperbolic tangent function given as below:

$$\rho_1 = \frac{tanh(\beta(\rho_f - \rho_\beta)) + tanh(\beta\rho_\beta)}{tanh(\beta(1-\rho_\beta)) + tanh(\beta\rho_\beta)}, \tag{9}$$

where ρ_1 is the projected density variable, β is the projection steepness and ρ_β is the projection point. Eventually, the classic "power law" is enforced to further suppress the occurrence of the grey region as follows:

$$\rho_{=}\rho_{min} + (1-\rho_{min})\rho_1^p, \tag{10}$$

where ρ_{min} is the lower bound of the density variable and set to be 0.001 to avoid numerical instability. p is the penalization factor and usually set to be 3. This ρ will be employed in the penalization of related physics quantities, i.e., thermal conductivity in this case in the following manner:

$$k = k_0 \cdot \rho, \tag{11}$$

where k_0 is the thermal conductivity for a solid material. This k will play a huge role in the solution process of equation (7) as it relates the physics quantity with the density variable, and further the shape and topology of the design at a given moment. The update of the design variable ρ is realized using the method of moving asymptotes (MMA) [30].

4 NUMERICAL EXAMPLES

In this section, two numerical examples will be provided to demonstrate the feasibility of the heat sink design principle. The first example deals with a benchmark 2D case, generating classic tree-like structures. The second example is dedicated to a heat sink design for a 3D integrated power converters. The volume fraction constraint is set to be 30% for all the provided examples. The solid material used in this study is aluminum with $k_{alu} = 166.9W/(m*K)$. The reference thermal convection coefficient $h_0 = 15W/(m^2*K)$. The ρ_l and ρ_u are 0.8 and 0.9, respectively. R_{min} in the Helmholtz filtering equation (8) is set to be 0.1cm for both numerical examples. In the projection scheme (see equation (9)), the projection steepness is given as $\beta = 8$ and the projection point is set to be $\rho_\beta = 0.5$.

4.1 A 2D Benchmark Heat Sink Design

The boundary condition for a 2D benchmark heat sink example is shown in Figure 2. The square is of dimension 10 cm $\times$ 10 cm. A boundary heat flux $q = 10W/m^2$ is located at the bottom center, mimicking the power generation from power device, e.g., CPU. All other boundaries are kept adiabatic. The square design domain is discretized using 10000 quadrilateral elements. The maximum element size is 0.1cm.

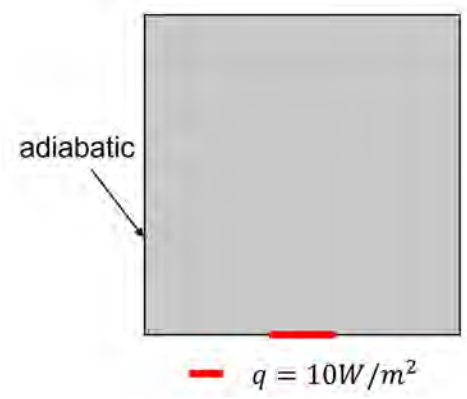

FIGURE 2: THE BOUNDARY CONDITION OF A 2D BENCHMARK HEAT SINK

The topology optimization result for Figure example 1 is displayed in Figure 3. The classic tree-like structure is produced to enhance the convection effect between solid material and air flow.

4.2 A 3D Heat Sink Design for Power Device

In this example, we try to optimize a heat sink design for a 3D integrated power stage (IPS). The IPS has been designed delicately to provide a higher power density with a more compact volume. This poses a challenge for the cooling system to timely dissipate the heat loss from such IPS to elongate its lifespan. A 3D IPS architecture is shown in Figure 4. The DC-DC stage is placed at the two sides of the heat sink region (grey block). Standing on top of the heat sink is the DC-AC stage, beneath the DC Link PCB. An effective and efficient heat sink design

FIGURE 3: THE OPTIMIZED STRUCTURE FOR EXAMPLE 1 WITH ONLY BOTTOM HEAT FLUX

conformal to the 3D IPS architecture in Figure 4. is sought after using the density-based topology optimization scheme.

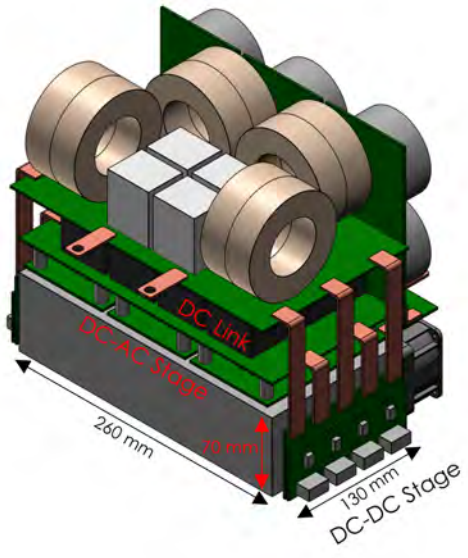

FIGURE 4: A 3D IPS ARCHITECTURE

The dimension for the heat sink design space is shown in Figure 5. All the dimensions are given in mm. The small square copper cells with a dimension of 16.5mm $\times$ 16.5mm $\times$ 0.5mm on top and two sides represent different heat source inputs. All other heat sink components are made of aluminum. A 8 mm thick wall is designated as the non-design region, as it is used to provide the mechanical withstanding functionality. The inner block with a dimension of 244mm $\times$ 130mm $\times$ 62mm is the actual design domain for the heat sink. According to our experiments, the direct topology optimization of the 3D models would be computationally intimidating. Also, the existence of multiple different thermal loads would run into some convergence issues. Here, we propose to design the 3D thermal cloak by extruding some representative 2D heat sink designs. The first representative 2D heat sink design is shown in Figure 3. This 2D design can be extruded to mimic the center region of the block design domain, where the main thermal load is from the top. A second representative 2D heat sink is shown in Figure 6, which is roughly resembling the side and top power inputs case in the corner region of the block design domain. The square design domain is also discretized using 10000 quadrilateral elements. The maximum element size is 0.1cm. The optimized heat sink design for the 2D representative cell with two side boundary fluxes is exhibited in Figure 7.

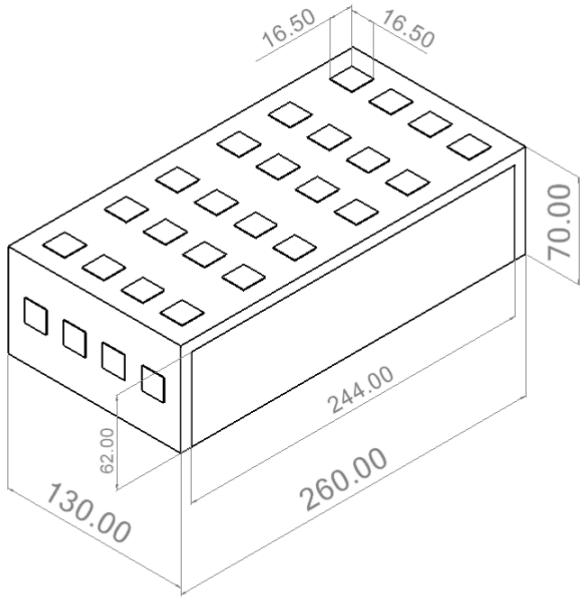

FIGURE 5: THE DIMENSION OF A 3D HEAT SINK

Once we obtain the two representative 2D heat sink designs, we can assembly their extrusions together (with minor scaling) to conformally fit into the block design domain with a dimension of 244mm $\times$ 130mm $\times$ 62mm. The assembled 3D heat sink for the IPS is shown in Figure 8. A zoom-in right side view of the 3D heat sink is given in Figure 9.

The performance of the optimized and assembled 3D heat sink designs are compared with two intuitive baseline designs. The boundary conditions for the 3D heat sink are reiterated with

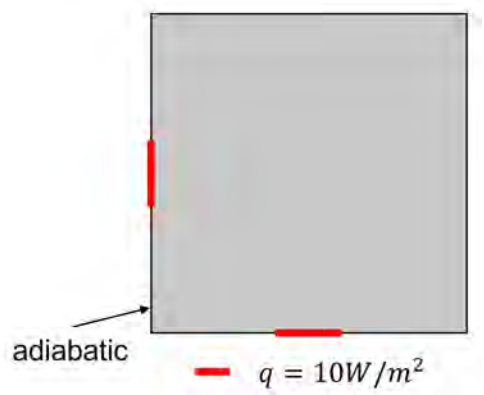

FIGURE 6: THE BOUNDARY CONDITION OF A 2D HEAT SINK WITH TWO SIDE HEAT FLUXES

FIGURE 7: THE OPTIMIZED STRUCTURE FOR EXAMPLE 2 WITH TWO SIDE HEAT FLUXES

details. As shown in Figure 10, the square cells in color with a dimension of 16.5mm $\times$ 16.5mm $\times$ 0.5mm are made of copper with $k_{cu} = 390W/(m*K)$. The light grey non-design region are composed of aluminum with $k_{alu} = 166.9W/(m*K)$. The dark grey region is the design space for the heat sink, where the aluminum will be distributed to dissipate the heat loss away from colored power inputs. A thermal contact resistance of $0.3K/W$ is applied to all the interface between the copper cells and aluminum outer surface. Since there will be fan blowing air from the right side as shown in Figure 4 (rear), the thermal convection coefficient h is set to be $100W/(m^2*K)$ for the surfaces inside the block design domain. For other exposed surface, a smaller convection coefficient $15W/(m^2*K)$ is assigned.

The simulated temperature distribution for the optimized heat sink is shown in Figure 11. The temperature profile shows correspondence to the boundary conditions, where the high temperatures occur at the heat sources (refers to Figure 10). The maximum and minimum temperature are 83.387 $^\circ C$ and 26.065

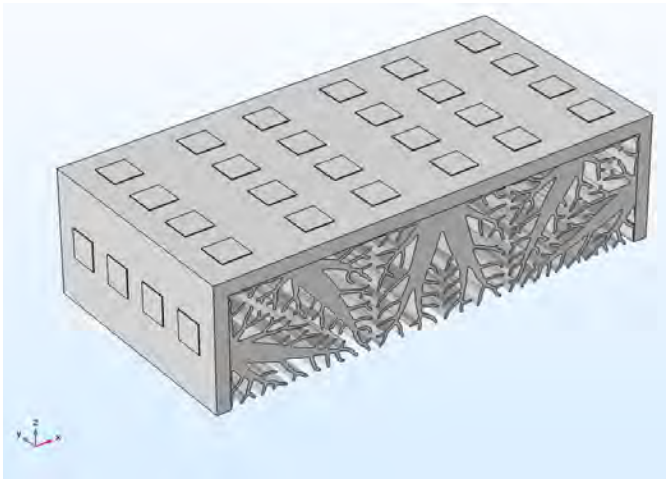

FIGURE 8: THE ASSEMBLED 3D HEAT SINK DESIGN FOR THE IPS

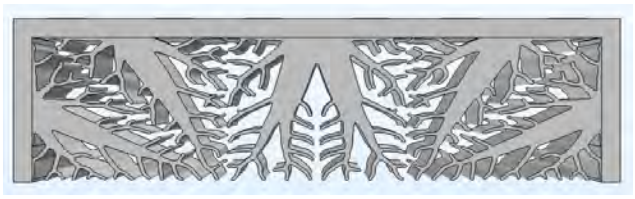

FIGURE 9: RIGHT SIDE VIEW OF THE ASSEMBLED 3D HEAT SINK DESIGN FOR THE IPS

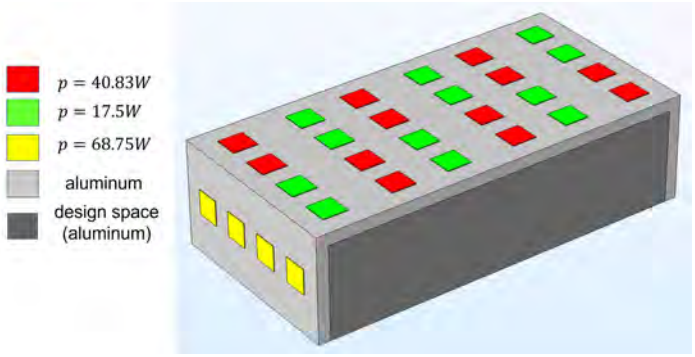

FIGURE 10: THE BOUNDARY CONDITIONS OF THE HEAT SINK DESIGN FOR THE IPS

$^\circ C$, respectively. Two reference designs with uniformly distributed cylindrical holes are shown in Figure 12 and 13. All the cylindrical holes share the same diameter 6mm. Baseline design 1 has 28 $\times$ 8 holes while baseline design 2 is drilled 22 $\times$ 6 holes. The highest and lowest temperature for baseline design 1 are 90.545 $^\circ C$ and 33.384 $^\circ C$, respectively. For baseline design 2, the two indexes will be 97.734 $^\circ C$ and 44.013 $^\circ C$, respectively. It

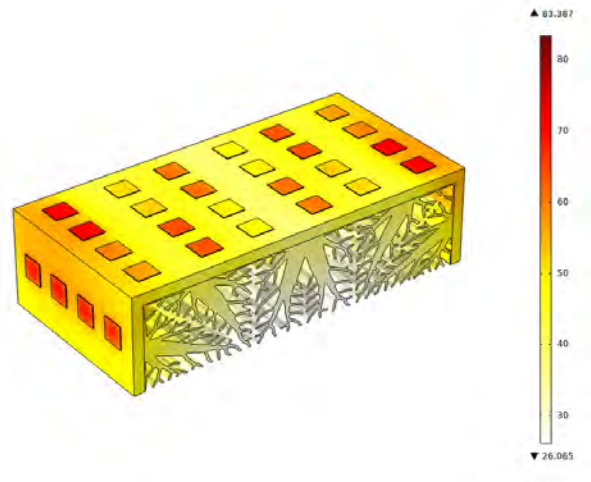

FIGURE 11: TEMPERATURE FIELD FOR THE OPTIMIZED HEAT SINK

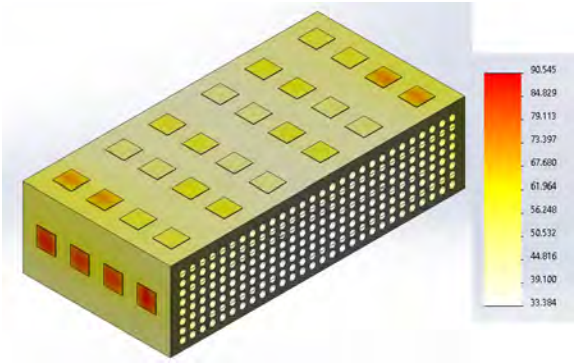

FIGURE 12: TEMPERATURE FIELD FOR THE CIRCULAR BASELINE DESIGN 1

is shown that the optimized heat sink outperforms the two baseline designs considerably.

5 CONCLUSION AND FUTURE WORK

In this study, we apply the density-based topology optimization method to design thermal heat sinks for power devices. The convection effect is taken into consideration by treating it as an equivalent volumetric integral term. Some numerical techniques are adopted to regularize the optimization problem and render a crisp "0-1" design. Two numerical examples are provided to demonstrate the feasibility of the proposed method. The first 2D benchmark example deals with a heat sink design with a single boundary flux. The classic tree-like structure is reproduced as shown in Figure 3. Then, a 3D heat sink, specially designed for an IPS architecture shown in Figure 4 , is tackled as the second

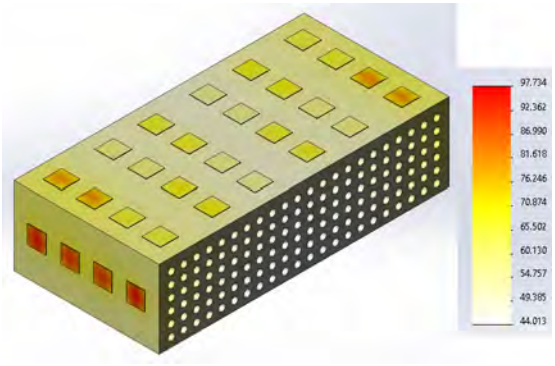

FIGURE 13: TEMPERATURE FIELD FOR THE CIRCULAR BASELINE DESIGN 2

numerical example. Due to the intimidating computational cost of directly solving the optimization problem on the 3D models, we propose to circumvent this hurdle by extruding some representative 2D heat sink design to conformally fit into the IPS architecture. This treatment might not be optimal, but it could at least provide some sub-optimal solutions. This point can be supported by the comparisons of the FEA with two baseline designs with varying number of holes with a fixed diameter. The optimized heat sink has a superior cooling performance compared with the two intuitive baseline designs.

However, some aspects can still be improved. First, the direct optimization on 3D models should be addressed in the future work, which is expected to provide a better cooling performance. Second, the topologically optimized heat sink for the IPS should be 3D printed and some practical experiments should be carried out to further validate the optimized thermal heat sink in the cooling performance of IPS.

ACKNOWLEDGMENT

The authors gratefully acknowledge financial support from the National Science Foundation (CMMI-1762287), the Ford University Research Program (URP) (Award No. 2017-9198R), and the State University of New York (SUNY) at Stony Brook.

REFERENCES

[1] Tummala, R. R., et al., 2001. "Fundamentals of microsystems packaging".

[2] Koga, A. A., Lopes, E. C. C., Nova, H. F. V., De Lima, C. R., and Silva, E. C. N., 2013. "Development of heat sink device by using topology optimization". *International Journal of Heat and Mass Transfer,* ***64***, pp. 759–772.

[3] Khattak, Z., and Ali, H. M., 2019. "Air cooled heat sink geometries subjected to forced flow: A critical review". *Inter-*

national Journal of Heat and Mass Transfer, ***130***, pp. 141–161.

[4] Shende, M. D., and Mahalle, A., 2013. "Cooling of electronic equipments with heat sink: a review of literature". *IOSR Journal of Mechanical and Civil Engineering (IOSR-JMCE),* ***5***(2).

[5] Alexandersen, J., Sigmund, O., and Aage, N., 2016. "Large scale three-dimensional topology optimisation of heat sinks cooled by natural convection". *International Journal of Heat and Mass Transfer,* ***100***, pp. 876–891.

[6] Bergman, T. L., Lavine, A. S., Incropera, F. P., and DeWitt, D. P., 2011. *Introduction to heat transfer*. John Wiley & Sons.

[7] Elghool, A., Basrawi, F., Ibrahim, T. K., Habib, K., Ibrahim, H., and Idris, D. M. N. D., 2017. "A review on heat sink for thermo-electric power generation: Classifications and parameters affecting performance". *Energy conversion and management,* ***134***, pp. 260–277.

[8] Xu, X., Wu, Y., Zuo, L., and Chen, S., 2021. "Topology optimization of multimaterial thermoelectric structures". *Journal of Mechanical Design,* ***143***(1).

[9] Xu, X., Wu, Y., Zuo, L., and Chen, S., 2019. "Multimaterial topology optimization of thermoelectric generators". In International Design Engineering Technical Conferences and Computers and Information in Engineering Conference, Vol. 59186, American Society of Mechanical Engineers, p. V02AT03A064.

[10] Hensler, A., Bigl, T., Neugebauer, S., and Pfefferlein, S., 2017. "Air cooled sic three level inverter with high power density for industrial applications". In PCIM Europe 2017; International Exhibition and Conference for Power Electronics, Intelligent Motion, Renewable Energy and Energy Management, VDE, pp. 1–8.

[11] Chen, C., Huang, Z., Chen, L., Tan, Y., Kang, Y., and Luo, F., 2018. "Flexible pcb-based 3-d integrated sic half-bridge power module with three-sided cooling using ultralow inductive hybrid packaging structure". *IEEE Transactions on Power Electronics,* ***34***(6), pp. 5579–5593.

[12] Dbouk, T., 2017. "A review about the engineering design of optimal heat transfer systems using topology optimization". *Applied Thermal Engineering,* ***112***, pp. 841–854.

[13] Xu, X., Chen, S., Gu, X. D., and Wang, M. Y., 2021. "Conformal topology optimization of heat conduction problems on manifolds using an extended level set method (x-lsm)". In International Design Engineering Technical Conferences and Computers and Information in Engineering Conference, Vol. 85390, American Society of Mechanical Engineers, p. V03BT03A030.

[14] Xu, X., Gu, X. D., and Chen, S., 2022. "Shape and topology optimization of conformal thermal control structures on free-form surfaces: A dimension reduction level set method (dr-lsm)". *Computer Methods in Applied Mechanics and Engineering,* ***398***, p. 115183.

[15] Dede, E. M., 2009. "Multiphysics topology optimization of heat transfer and fluid flow systems". In proceedings of the COMSOL Users Conference.

[16] Dede, E. M., Joshi, S. N., and Zhou, F., 2015. "Topology optimization, additive layer manufacturing, and experimental testing of an air-cooled heat sink". *Journal of Mechanical Design,* ***137***(11).

[17] Alexandersen, J., Aage, N., Andreasen, C. S., and Sigmund, O., 2014. "Topology optimisation for natural convection problems". *International Journal for Numerical Methods in Fluids,* ***76***(10), pp. 699–721.

[18] Joo, Y., Lee, I., and Kim, S. J., 2017. "Topology optimization of heat sinks in natural convection considering the effect of shape-dependent heat transfer coefficient". *International Journal of Heat and Mass Transfer,* ***109***, pp. 123–133.

[19] Zeng, S., Kanargi, B., and Lee, P. S., 2018. "Experimental and numerical investigation of a mini channel forced air heat sink designed by topology optimization". *International Journal of Heat and Mass Transfer,* ***121***, pp. 663–679.

[20] Li, H., Ding, X., Meng, F., Jing, D., and Xiong, M., 2019. "Optimal design and thermal modelling for liquid-cooled heat sink based on multi-objective topology optimization: An experimental and numerical study". *International Journal of Heat and Mass Transfer,* ***144***, p. 118638.

[21] Lei, T., Alexandersen, J., Lazarov, B. S., Wang, F., Haertel, J. H., De Angelis, S., Sanna, S., Sigmund, O., and Engelbrecht, K., 2018. "Investment casting and experimental testing of heat sinks designed by topology optimization". *International Journal of Heat and Mass Transfer,* ***127***, pp. 396–412.

[22] Bendsøe, M. P., and Kikuchi, N., 1988. "Generating optimal topologies in structural design using a homogenization method". *Computer methods in applied mechanics and engineering,* ***71***(2), pp. 197–224.

[23] Bendsøe, M. P., 1989. "Optimal shape design as a material distribution problem". *Structural optimization,* ***1***(4), pp. 193–202.

[24] Zhou, M., and Rozvany, G., 1991. "The coc algorithm, part ii: topological, geometrical and generalized shape optimization". *Computer Methods in Applied Mechanics and Engineering,* ***89***(1-3), pp. 309–336.

[25] Sigmund, O., and Maute, K., 2013. "Topology optimization approaches". *Structural and Multidisciplinary Optimization,* ***48***(6), pp. 1031–1055.

[26] Yoon, M., and Koo, B., 2019. "Topology design optimization of conductive thermal problems subject to design-dependent load using density gradients". *Advances in Mechanical Engineering,* ***11***(5), p. 1687814019850735.

[27] Lee, G., Joo, Y., and Kim, S. J., 2021. "On the objective

function for topology optimization of heat sinks". *IEEE Transactions on Components, Packaging and Manufacturing Technology,* ***11***(11), pp. 1776–1782.

[28] Lazarov, B. S., and Sigmund, O., 2011. "Filters in topology optimization based on helmholtz-type differential equations". *International Journal for Numerical Methods in Engineering,* ***86***(6), pp. 765–781.

[29] Wang, F., Lazarov, B. S., and Sigmund, O., 2011. "On projection methods, convergence and robust formulations in topology optimization". *Structural and multidisciplinary optimization,* ***43***(6), pp. 767–784.

[30] Svanberg, K., 1987. "The method of moving asymptotes—a new method for structural optimization". *International journal for numerical methods in engineering,* ***24***(2), pp. 359–373.